Penerbit Akademia Baru

Journal of Advanced Research in Micro and Nano Engineering

Journal homepage: https://akademiabaru.com/submit/index.php/armne
ISSN: 2756-8210

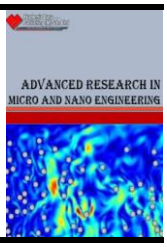

Mixed Convection Hybrid Nanofluid Flow past a Stagnation-Point Region with Variable Viscosity and Second-Order Slip

Shahirah Abu Bakar[1,*], Norihan Md Arifin[2,3], Ioan Pop[4]

[1] Takasago Thermal/Engineering Systems Laboratory, Malaysia-Japan International Institute of Technology, Universiti Teknologi Malaysia, 54100, Kuala Lumpur, Malaysia
[2] Institute for Mathematical Research, Universiti Putra Malaysia, 43400, UPM Serdang, Selangor, Malaysia
[3] Department of Mathematics & Statistics, Faculty of Science, Universiti Putra Malaysia, 43400, UPM Serdang, Selangor, Malaysia
[4] Department of Mathematics, Babes-Bolyai University, R-40084 Cluj-Napoca, Romania

ABSTRACT

The objective of this study is to investigate the effects of mixed convection flow dispersed with a hybrid nanofluid over a permeable shrinking surface past a stagnation-point region considering the influence of second-order velocity slip and variable viscosity on the flow behaviour. For the hybrid nanofluid, water (H_2O) is chosen to be the base fluid, while silver (Ag) decorated copper oxide (CuO) nanoparticles are employed as the hybrid component. To achieve the mathematical model, a suitable method of similarity transformation is applied to convert the partial differential equations (PDEs) model into a system of non-linear ordinary differential equations (ODEs). The shooting technique method and bvp4c solver in MAPLE and MATLAB are employed to obtain the analytical solutions of the mathematical model. The obtained results, including the impacts of variable viscosity, second-order velocity slip, mixed convection parameter, suction, shrinking parameter, and nanofluid volume fraction, are presented through tables and figures. The study reveals the existence of dual solutions (upper and lower branches) prior to shrinking sheet $\lambda < 0$. Furthermore, the thermal distribution exhibits mixed behaviours with respect to the variable viscosity number and second-order slip parameter, while demonstrating an increase with the presence of Ag-ϕ_1. The velocity distribution experiences an enhancement with both ϕ_1 concentration and variable viscosity number. Stability analysis is then employed and shows that the first branch is stable, whereas the second branch exhibits an opposite outcome.

Keywords:
Hybrid nanofluid; mixed convection; second-order velocity slip; variable viscosity; dual solutions; stability analysis

Received: 11 Feb. 2023 **Revised: 20 Apr. 2023** **Accepted: 15 May 2023** **Published: 25 May 2023**

1. Introduction

In modern times, there is a growing interest in exploring various methods to enhance heat transfer efficiency, including modifying boundary conditions, flow geometry, or the thermal conductivity of the fluid. However, one significant challenge is that larger suspended particles may lead to issues such as erosion and clogging in microchannels. To overcome these limitations, researchers have turned to smaller-sized particles, known as nanoparticles, as seen in the case of

* *Corresponding author*
Email address: shahirah.abubakar@utm.my

https://doi.org/10.37934/armne.12.1.121

nanofluids. Nanofluids are specifically designed to improve the thermal conductivity of base fluids like water, ethylene glycol, and kerosene, among others. In the realm of nanofluids, a wide range of nanoparticles, including copper, oxides, carbides, nitrites, and other chemically stable materials, have been generated. These materials exhibit unique chemical and physical properties when reduced to nanometer-size. One of the features of nanofluids is their smooth flow through microchannels without clogging, resembling the behaviour of liquid molecules. A seminal study by Choi and Eastman [1] demonstrated that incorporating a small quantity of nanoparticles into a fluid system can effectively double its thermal conductivity performance. This characteristic then has garnered significant attention and research efforts in the field of heat transfer studies.

Further, the combination of two nanoparticles or known as hybrid nanofluid has garnered significant attention from researchers due to its profound impact in various industries. This innovative approach holds immense potential for applications in automobile or aircraft engines coolants, microfluidics systems and lab-on-a-chip devices, fabricate nanocomposite materials, medical lubrication, and solar heating. The main motivation behind this combination is to overcome the individual weaknesses exhibited by each nanoparticle, such as alumina (Al_2O_3) boasts excellent chemical inertness and stability but has a relatively lower thermal conductivity (k = 40). On the other hand, metallic nanoparticles such as silver (Ag) and graphene exhibit significantly higher thermal conductivities (Ag with k = 429, graphene with k = 3000). By combining Ag and Al_2O_3, for instance, the limitations of Al_2O_3 can be offset and leading to improved performance. A carefully designed composition of two nanoparticles can balance out vulnerabilities and enhance each other's positive properties. This approach not only enhances physical properties, but also helps minimize production costs. Suresh *et al.,* [2] elaborated on the hybrid Cu- Al_2O_3/water nanofluid and its thermophysical properties using a two-step method, presenting a new concept in nanomaterial design that positively impacted mechanical and thermal properties. Devi and Devi [3] explored the effect of suction in Cu-Al_2O_3/water flow over a stretching sheet with hydromagnetic effects. A study of nonlinear radiation and variable thermal conductivity on a permeable surface of hybrid Cu-Al_2O_3/water nanofluid was intensively examined by Usman *et al.,* [4]. Afridi *et al.,* [5] then studied entropy generation and thermal dissipation over a curved surface with hybrid nanofluid flow, while Yahaya *et al.,* [6] performed a study of - hybrid nanofluid flow past a permeable stretching and shrinking sheets. Bakar *et al.,* [7] reported a higher percentage of hybrid nanofluid performance on the heat transfer rate at 36.73% compared to the percentage of mono-nanofluid at 27.35%, indicating the rate increment at 9.38%. Their study also revealed the increasing numbers of nanoparticles volume fraction is showed to enhance both solutions of the boundary layer flow as shrinking parameter is possessed to execute dual solutions in their study. Recent studies on hybrid nanofluid flow also have been extensively analysed by Abbas *et al.,* [8], Gul *et al.,* [9], Hussain *et al.,* [10], Muhammad *et al.,* [11] and Rashidi *et al.,* [12].

Mixed convection is a significant mechanism in heat transfer, drawing interest in various technological, industrial, and natural applications. It involves the combined effects of natural and forced convections, making it a general case when a flow is influenced by both inner volumetric forces and an outer forcing system. In the context of previous studies, Hussain *et al.,* [13] explored that Richardson number improves the mixed convection modes as well as the entropy generation tools and heat transfer rate. Jarray *et al.,* [14] studied the mixed convection of hybrid Ag-MgO-water nanofluid flow in a porous horizontal channel and it is occurred that the size and intensities of mixed convection roll-cells increase by Darcy number and decline by nanoparticle volume fractions. Rostami *et al.,* [15] explained that the opposing flow of silicon dioxide (SiO_2) and aluminium oxide (Al_2O_3) reduced the velocity and thermal boundary layer thicknesses compared to forced convection and opposing flow of hybrid nanofluid, while a report of mixed convection flow of hybrid nanofluid near

the stagnation point over a curved surface by Khan *et al.,* [16] captivated the nanoparticle volume fraction of SiO_2-Al_2O_3 improves the skin friction coefficient and Nusselt number rapidly. In a study by Zainal et *al.,* [17], they identified that the mixed convection parameter λ possessed dual solutions. The boundary layer separation occurred in the opposing flow regime, and the nanoparticle volume fraction increased the velocity distribution simultaneously. Several other researchers have also explored mixed convection flow with hybrid nanofluids, including Elsaid and Abdel-Wahed [18], Khashi'ie *et al.,* [19], Patil and Kurkani [20], Rosca *et al.,* [21], Gohar *et al.,* [22], Xia *et al.,* [23], among others.

Fluid dynamics encompasses the study of velocity slip, which occurs in the vertical flow of two-phase mixtures when there is a difference in velocities between solids and liquids due to slip at the interface. Slip factor in boundary condition is considered significance as it employed in modern technologies and machineries, such as the conventional slip factor model for impeller discharge, where impeller is a rotor used to increase the pressure and flow of a fluid. The degree of slip at the boundary conditions is influenced by various interfacial parameters, including liquid densities, liquid-solid coupling strength, and thermal interface roughness, as stated by Zhu *et al.,* [24]. Later, the concept of second-order velocity slip arises from the breakdown of Navier's slip condition under higher shear rates, leading to a rapid increase in slip length. While the slip condition at the boundary worked well at a sufficiently low shear rates, second-order velocity slip is found to be crucial in fluid flow. Zhu *et al.,* [25] discovered that the first-order velocity slip reduces the boundary layer thickness, while the second-order velocity slip acts in the opposite direction. Rosca *et al.,* [26] investigated mixed convection stagnation point flow past a vertical plate. Their results confirmed a decrement in the skin friction coefficient with both first and second-order velocity slips until a certain value of the mixed convection parameter was reached. Yan *et al.,* [27] later confirmed that the higher number of velocity slip factor attributed in the decrement of skin friction coefficient. The thermal slip factor, however, does not affect the separation of boundary layer. Further, Tulu and Ibrahim [28] stated in their study of natural convection flow with hybrid nanofluid, second-order velocity slip and variable viscosity over a stretching surface that the second-order slip condition played a physical occurrence in the fluid flow where the thermal boundary layer grows, while the momentum boundary layer lessens. In this recent year, other studies in hybrid nanofluid flow with second-order slip condition are made accessible such as by Waini *et al.,* [30], Gul *et al.,* [30], Abu Bakar *et al.,* [31], Botmart *et al.,* [32], Lone *et al.,* [33], Asghar *et al.* [34], to name a few.

2. Mathematical Modelling

2.1 Properties of Fluids and Nanofluids

This current study utilizes Ag-CuO/water as the hybrid nanofluid form. The study explores a range of nanoparticle volume fractions ϕ, with the volume of Ag (ϕ_1) varying between $1\% \leq \phi_1 \leq 4\%$ and CuO's (ϕ_2) volume fraction is between $1\% \leq \phi_2 \leq 5\%$. The volume fraction for the hybrid nanofluid follows the formulation presented in the work of Xie *et al.,* [35]

$$\phi_{hnf} = \phi_1 + \phi_2 = \frac{V_{Ag}+V_{CuO}}{V_{Ag-CuO}}.$$

To frame the thermophysical properties, we followed the one suggested by Takabi and Salehi [36] and Ghalambaz *et al.,* [37] as listed in Table 1, while Table 2 presented the values of nanoparticles properties. Here, the thermophysical characteristics of the fluid is represented at 25ºC and the viscosity coefficient of the fluid μ_f, is constituted to vary as an inverse function of temperature, which is given by Reynolds exponential viscosity model as $\mu_f = \mu_0 e^{-B_1\theta(\eta)}$, see Manjunatha *et al.,* [38] and

Venkateswarlu and Satya Narayana [39], where B_1 is the coefficient of variable viscosity. The definition of ρ, k, β and C_p are density, thermal conductivity, thermal expansion and heat capacitance, respectively, where the subscript of *f, nf* and *hnf* represent fluid, nanofluid and hybrid nanofluid, accordingly.

Table 1
Correlation properties of hybrid nanofluid, see Abu Bakar *et al.,* [31], Takabi and Salehi [36] and Ghalambaz *et al.,* [37]

Properties	Hybrid nanofluid correlations
Viscosity	$\mu_{hnf} = \frac{\mu_f}{(1-\phi_1)^{2.5}(1-\phi_2)^{2.5}}$
Heat capacity	$(\rho C_p)_{hnf} = (1-\phi_2)\left[(1-\phi_1)(\rho C_p)_f + \phi_1(\rho C_p)_1\right] + \phi_2(\rho C_p)_2$
Thermal expansion coefficient	$(\rho\beta)_{hnf} = (1-\phi_2)\left[(1-\phi_1)(\rho\beta)_f + \phi_1(\rho\beta)_1\right] + \phi_2(\rho\beta)_2$
Density	$\rho_{hnf} = (1-\phi_2)\left[(1-\phi_1)\rho_f + \phi_1\rho_1\right] + \phi_2\rho_2$
Thermal conductivity	$\frac{k_{hnf}}{k_{nf}} = \frac{k_2+2k_{nf}-2\phi_2(k_{nf}-k_2)}{k_2+2k_{nf}+\phi_2(k_{nf}-k_2)}$ where $\frac{k_{nf}}{k_f} = \frac{k_1+2k_{nf}-2\phi_1(k_f-k_1)}{k_1+2k_f+\phi_1(k_f-k_1)}$

Table 2
Thermophysical properties for selected nanoparticles

Physical Properties	Density, ρ (kg/m^3)	Specific heat, C_p (J/kgK)	Thermal conductivity, k (W/mK)
Water	997.1	4179	0.613
Ag	10500	235	429
CuO	6320	531.8	76.5
Cu	8933	385	401

2.2 Formulation of Mathematical Modelling

In this study, we consider the two-dimensional stagnation point flow of a hybrid nanofluid with mixed convection flow, second-order velocity slip and variable viscosity past a permeable shrinking surface, as employed in Figure 1. To frame the configuration coordinate, the *x*-axis extends along the sheet surface while *y*-axis is measured to the normal surface. We also assume that the nanoparticle shape is in spherical form and the nanoparticle size is uniform. The surface velocity is modulated by the expression $U_w(x) = cx$, where *c* represents the plate velocity coefficient. Notably, *c* distinguishes between a shrinking plate at $c < 0$, and a stretching plate at $c > 0$. The dispersion of nanoparticles within the base fluid is presumed to attain thermal equilibrium, where the temperature of the fluid beneath the sheet is denoted as T_w, while T_∞ represents ambient temperature. It is assumed that the hybrid nanofluid exhibit stability as a composite, thereby rendering any concerns regarding agglomeration inconsequential. Further, the desired governing equations can be written as follows

$$\frac{\partial u}{\partial x} + \frac{\partial v}{\partial y} = 0, \tag{1}$$

$$\rho_{hnf}\left(u\frac{\partial u}{\partial x} + v\frac{\partial u}{\partial y}\right) = \mu_{hnf}T\frac{\partial^2 u}{\partial y^2} + (\rho\beta)_{hnf}(T-T_w)g + U_\infty\frac{\partial U_\infty}{\partial x}\rho_{hnf}, \tag{2}$$

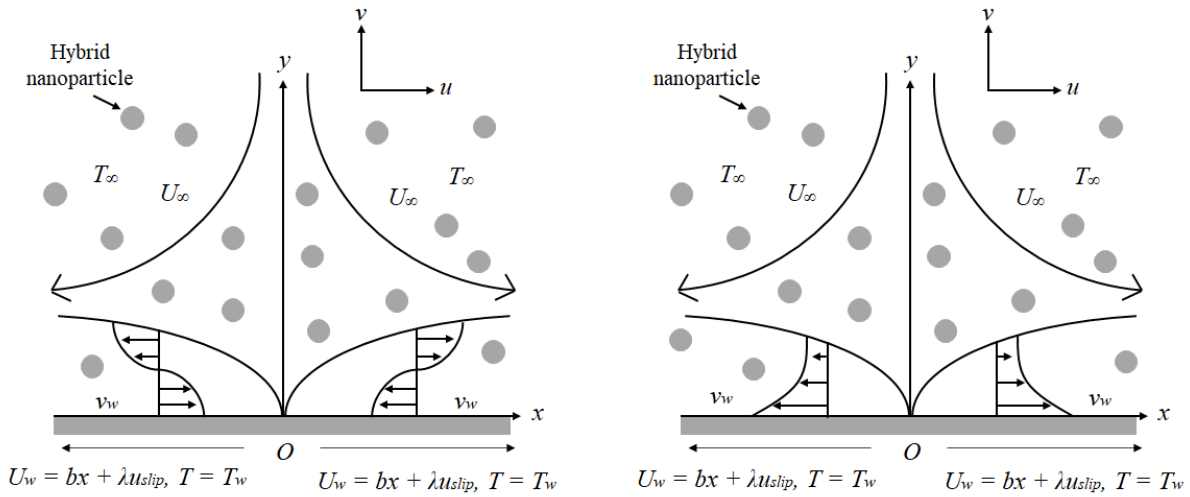

(a) Shrinking sheet when $\lambda < 0$ (b) Stretching sheet when $\lambda > 0$

Fig. 1. *Visual representation of shrinking and stretching sheets with hybrid nanofluid*

$$u\frac{\partial T}{\partial x} + v\frac{\partial T}{\partial y} = \frac{k_{hnf}}{(\rho C_p)_{hnf}}\frac{\partial^2 T}{\partial y^2} + \frac{\mu_{hnf}}{(\rho C_p)_{hnf}}T\left(\frac{\partial u}{\partial y}\right)^2, \tag{3}$$

subjected to the boundary conditions at

$$u = U_w(x) = cx + u_{slip}, v = v_w, T = T_w \text{ at } y \to 0$$
$$u \to 0, T \to T_\infty \text{ as } y \to \infty \tag{4}$$

From Eq. (1)-(4), *u* and *v* are the velocities of *x*- and *y*-axis direction, *T* is temperature, *g* is gravity, $U_\infty = bx$ is the velocity of the inviscid from the plate where *b* is positive constant and u_{slip} is slip velocity as proposed by Wu [40] and Acharya *et al.,* [41] which is defined by

$$u_{slip} = \left(\frac{2}{3}\frac{3-\alpha_1 m^3}{\alpha_1} - \frac{1-m^2}{K_n}\right)\omega\frac{\partial u}{\partial y} - \left(\frac{m^4}{4} + \frac{1-m^2}{2K_n^2}\right)\omega^2\frac{\partial^2 u}{\partial y^2} = A_1\frac{\partial u}{\partial y} + A_2\frac{\partial^2 u}{\partial y^2}, \tag{5}$$

where α_1 is the coefficient of momentum accommodation, ω is molecule free mean path, $\mathrm{K_n} = \frac{\omega}{\mathrm{m}}$ is the local Knudsen number, $\mathrm{A_1} = \frac{2}{3}\frac{3-\alpha_1 \mathrm{m}^3}{\alpha_1} - \frac{1-\mathrm{m}^2}{\mathrm{K_n}}$ is the first-order slip coefficient and $\mathrm{A_2} = \frac{\mathrm{m}^4}{4} + \frac{1-\mathrm{m}^2}{2\mathrm{K_n^2}}$ is the second-order slip coefficient. Higher-order terms, such as third-order or fourth-order velocity slips have not been considered as the primary objective of our study is to assess the accuracy and validity of the approximation for these first and second-order slips in the context of our respective fluid flow. By excluding higher-order slip terms, we can focus on the fundamental contributions of first and second-order slips to better understand their practical implications and applicability in real-world scenarios.

To deduce the PDEs in Eq. (1)-(3), the following dimensionless variables are introduced by

$$u = cx\, f'(\eta), v = -\sqrt{c\nu_f}f(\eta), \theta = \frac{T-T_\infty}{T_w-T_\infty}, \eta = y\sqrt{\frac{c}{\nu_f}}, \tag{6}$$

where Eq. (1) is satisfied, and Eq. (2) and (3) can simplified to

$$(1 - B\theta)D_1 f''' + D_2 \xi\theta + ff'' - (f')^2 + 1 = 0, \tag{7}$$

$$D_3\theta'' + \frac{(1-B\theta)}{D_4}(f'')^2 + Pr\, f\, \theta' = 0. \tag{8}$$

The boundary limitation in Eq. (4) can imposed to

$$f(0) = S, f'(0) = \lambda + L_1 f''(0) + L_2 f'''(0), \theta'(0) = 0 \text{ when } \eta = 0$$
$$f'(\eta) \to 1, \theta(\eta) \to 0 \text{ as } \eta \to \infty \tag{9}$$

Here, ξ is mixed convection parameter where $\xi > 0$ represents assisting flow and $\xi < 0$ denotes opposing flow, *B* is variable viscosity parameter, *Pr* is Prandtl number, *S* is suction parameter, λ is stretching/shrinking parameter with $\lambda < 0$ and $\lambda > 0$ are shrinking sheet and stretching sheet, respectively. Further, we have first-order velocity slip represented by L_1 while L_2 is second-order velocity slip. The description of these parameters, together with D_1, D_2, D_3 and D_4 are described as regards

$$D_1 = \frac{\mu_{hnf}/\mu_f}{\rho_{hnf}/\rho_f}, D_2 = \frac{(\rho\beta)_{hnf}/(\rho\beta)_f}{\rho_{hnf}/\rho_f}, D_3 = \frac{k_{hnf}/k_f}{(\rho C_p)_{hnf}/(\rho C_p)_f}, D_4 = (1-\phi_1)^{2.5}(1-\phi_2)^{2.5},$$
$$S = -\frac{v_w}{\sqrt{cv_f}}, \xi = \frac{Gr_x}{Re_x}, L_1 = A_1\sqrt{\frac{c}{\nu_f}}, L_2 = A_2\sqrt{\frac{c}{\nu_f}}, Pr = \frac{\nu_f(\rho C_p)_f}{k_f}, \tag{10}$$

where Re_x is local Reynolds number and Gr_x is Grashof number, which denoted by

$$Re_x = \frac{U_w(x)x}{\nu_f}, \mathrm{Gr}_x = \frac{(T_w - T_\infty)g\beta_f x^3}{\nu_f^2}. \tag{11}$$

The physical quantities of interest refer to the specific parameters or properties that are being studied, measure, or analysed in scientific research. Physical quantities of interest that convey the essential data for engineers to design apparatus by utilising hybrid nanoparticles are the coefficient of skin friction C_f and Nusselt number Nu_x. Following Aly and Pop [42], these quantities are assumed to be frame at the lower surface of the plate and can be written in the form of

$$C_f = \frac{\tau_w}{\rho_f U_w^2(x)}, Nu_x = \frac{xq_w}{k_f(T_w - T_\infty)}, \tag{12}$$

where $\tau_w = -\mu_{hnf}\left.\frac{\partial u}{\partial y}\right|_{y=0}$ and $q_w = -k_{hnf}\left.\frac{\partial T}{\partial y}\right|_{y=0}$ are shear stress along the plate and heat flux from the plate, accordingly. By employing the similarity variables in Eq. (6), the reduced form of C_f and Nu_x can finalised to

$$C_f\sqrt{Re_x} = \frac{1}{D_4}f''(0), Nu_x\frac{1}{\sqrt{Re_x}} = -D_5\theta'(0), \tag{13}$$

where $D_5 = \frac{k_{hnf}}{k_f}$.

2.3 Procedure of Numerical Approach

The ODEs presented in Eq. (7) and (8) with the corresponding boundary conditions in Eq. (9) are numerically solved using the shooting technique in MAPLE software. Shooting technique is a numerical approach that transforms a boundary value problem into an initial value problem (IVP). By utilizing MAPLE software for the numerical computations, the study can efficiently explore the behaviour of the system under different conditions, such as varying nanoparticle volume fractions and slip parameters. Bakar *et al.,* [7] and Abu Bakar *et al.,* [43] stated that this transformation involves iteratively "shooting" trajectories in different directions until the trajectory that satisfies the boundary value problem is obtained. In this process, variables are labelled according to a predefined scheme, streamlining the solution process such as

$$f = y_1, f' = y_1' = y_2, f'' = y_2' = y_3,$$
$$\theta = y_4, \theta' = y_4' = y_5.$$

Hence, the ODEs in Eq. (6) and (7) can formulated into

$$y_1' = y_2, y_2' = y_3,$$
$$y_3' = \frac{(y_2)^2 - y_1 y_3 - 1 - D_2 \xi y_4}{D_1(1 - B y_4)}$$
$$y_4' = y_5, y_5' = \frac{-Pr\, y_1\, y_5}{D_3} - \frac{(1 - B y_4)(y_3)^2}{D_3 D_4}.$$

Initially, the values are selective to be guessed when the initial conditions are not given. In condition of $\eta \to \infty$ at each parameter, the end of boundary layer region is determined when the unknown boundary layer values are fixed with the consecutive iterative step length is less than 10^{-6}.

3. Results and Discussions

Prior to our mathematical models in Eq. (7) and (8), a comparison between current and published results by Waini *et al.,* [44] and Bachok *et al.,* [45] has been analysed as presented in Table 3. Here, a good consensus is achieved where further outputs can be distinguished, accordingly.

Table 3
Comparison of skin friction coefficient $C_f\sqrt{Re_x}$ against λ and Cu-volume

λ	ϕ_1	$C_f\sqrt{Re_x}$		
		Present outcome	Waini *et al.,* [44]	Bachok *et al.,* [45]
-0.5	0.05	1.8855299	1.8855	-
	0.1	2.2865004	2.2865	2.2865
	0.2	3.1825937	3.1825	3.1826
0.0	0.05	1.5539410	1.5539	-
	0.1	1.8843336	1.8843	1.8843
	0.2	2.6226792	2.6227	2.6226

Figure 2(a) and 2(b) illustrated the impact of CuO-nanoparticle ϕ_2 against shrinking parameter λ on skin friction coefficient $C_f\sqrt{Re_x}$ and Nusselt number $Nu_x\frac{1}{\sqrt{Re_x}}$, where a non-unique solution is observed within a range of $\lambda_c \leq \lambda < 0$. The non-unique solution has led to the bifurcation of the solution branches into two distinct paths, commonly referred to as the first and second solutions (or first and second branches). When a non-linear system has multiple solutions for a given set of boundary conditions, the system's behaviour can diverge into different trajectories. Each branch represents a distinct solution and may possess unique characteristics and behaviours. In this study, the solution is pertinent into a peak of λ_c, where λ_c is the critical value of a solution. In Figure 2, both fluid flow and heat transfer rate are significantly expanded against $1\% \leq \phi_2 \leq 5\%$ and this increment indicating that the nanoparticle volumetric fraction is pressed in the wall direction when the viscosity of the buoyancy forces increases. Further, the effect of second-order velocity slip L_2 on skin friction coefficient $C_f\sqrt{Re_x}$ and Nusselt number $Nu_x\frac{1}{\sqrt{Re_x}}$ are visualised in Figure 3(a) and 3(b), accordingly, and it is clearly indicated that both boundary layer thicknesses and thermal transmittance rate are improving according to the numbers of L_2.

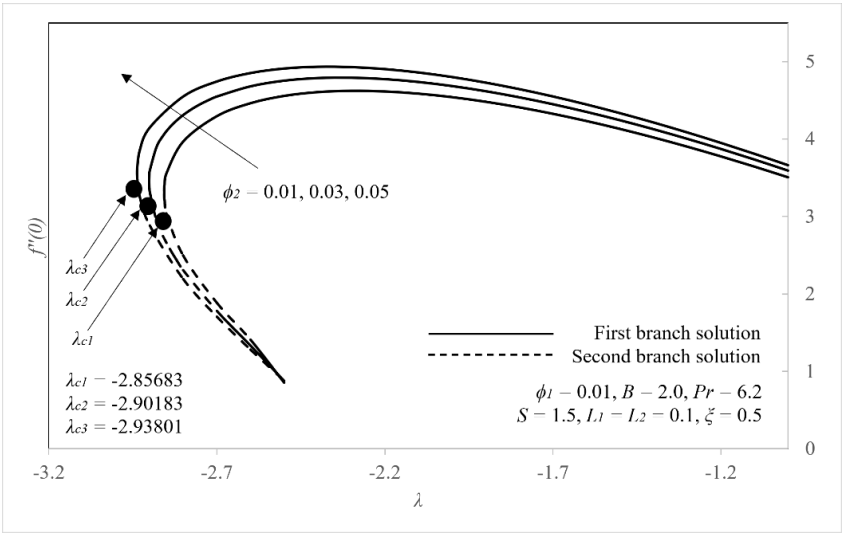

(a) Skin friction coefficient $C_f Re_x^{1/2}$

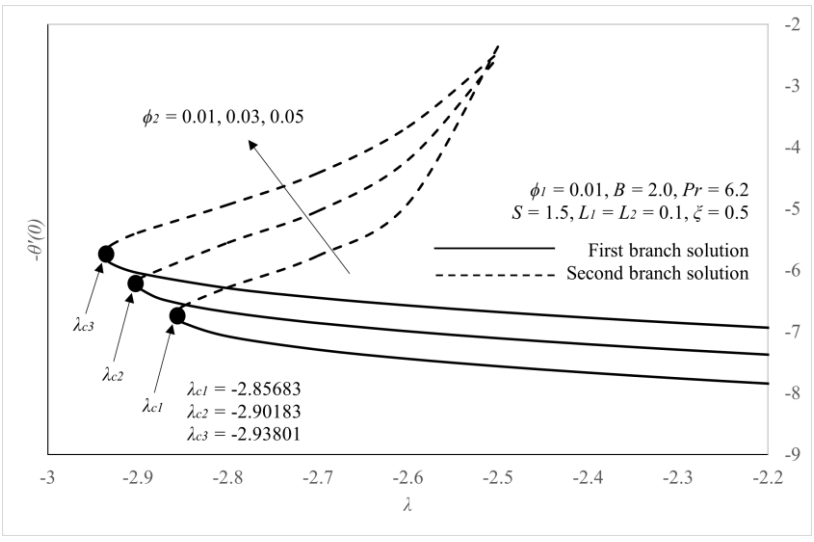

(b) Nusselt number $Nu_x\, Re_x^{-1/2}$

Fig. 2. Impact of CuO-ϕ_2 on $C_f Re_x^{1/2}$ and $Nu_x Re_x^{-1/2}$

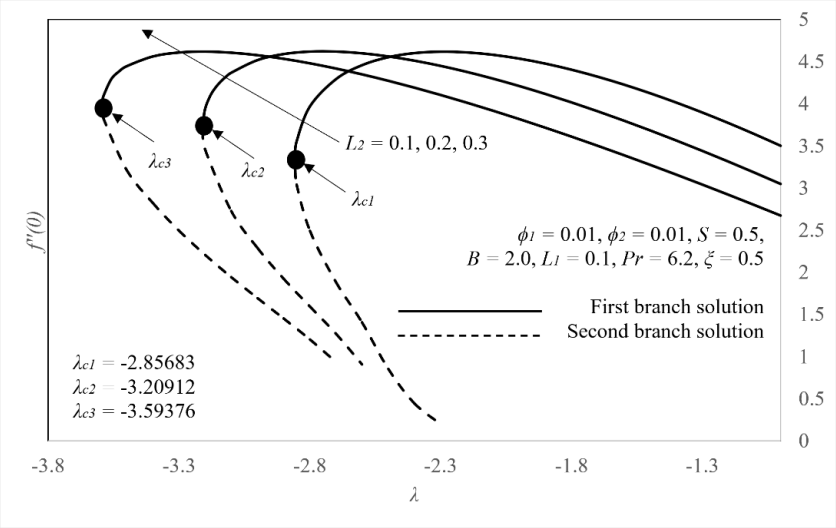

(a) Skin friction coefficient $C_f\ Re_x^{1/2}$

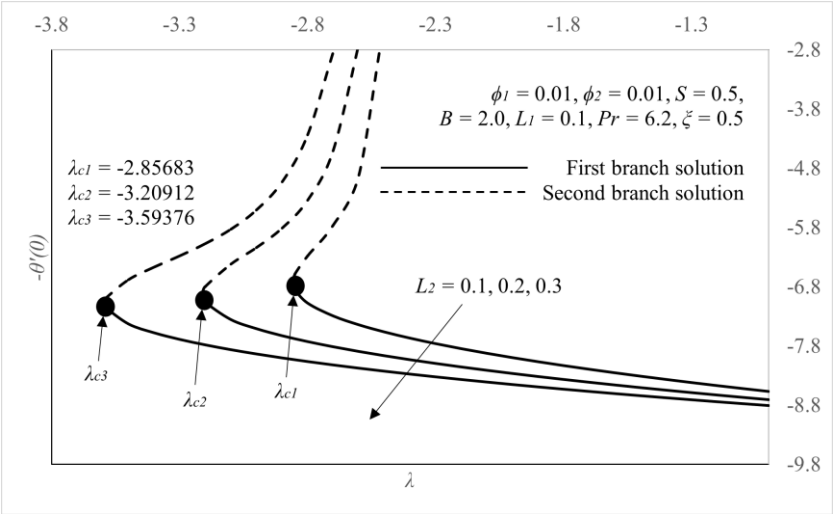

(b) Nusselt number $Nu_x Re_x^{-1/2}$

Fig. 3. Impact of L_2 coefficient on $C_f\ Re_x^{1/2}$ and $Nu_x Re_x^{-1/2}$

Dual solutions of the skin friction coefficient $C_f Re_x^{1/2}$ and Nusselt number $Nu_x Re_x^{-1/2}$ with respect to the suction parameter *S*, are prominently highlighted in Figure 4(a) and 4(b). These figures depict the behaviour of $C_f Re_x^{1/2}$ and $Nu_x Re_x^{-1/2}$ as the suction parameter varies. Similar to the patterns in Figure 2 and 3, an increase in the critical point λ_c with *S* signifies a significant expansion in the boundary layer thicknesses and heat transfer rate. This expansion can be attributed to the loss of friction when the boundaries of fluid and solid move in a simultaneous velocity at the fluid-solid interface. Additionally, it reflects the combined effects of the shrinking sheet's strength and the suction effect at the surface.

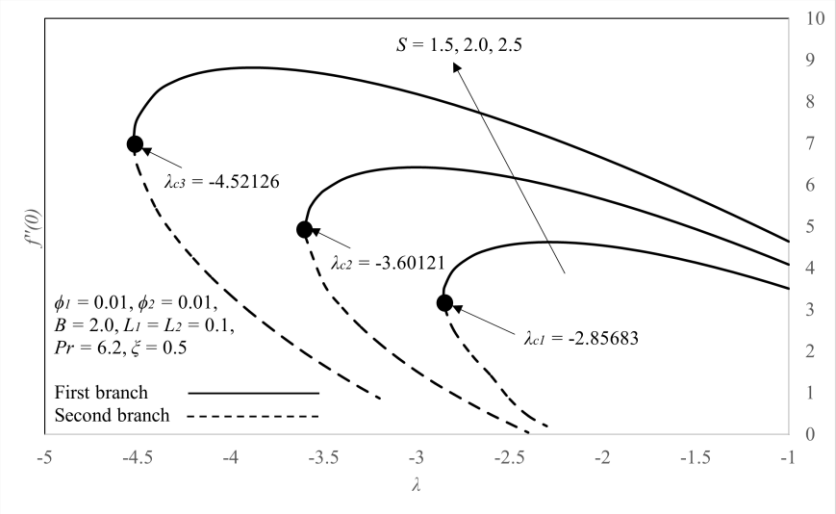

(a) Skin friction coefficient $C_f Re_x^{1/2}$

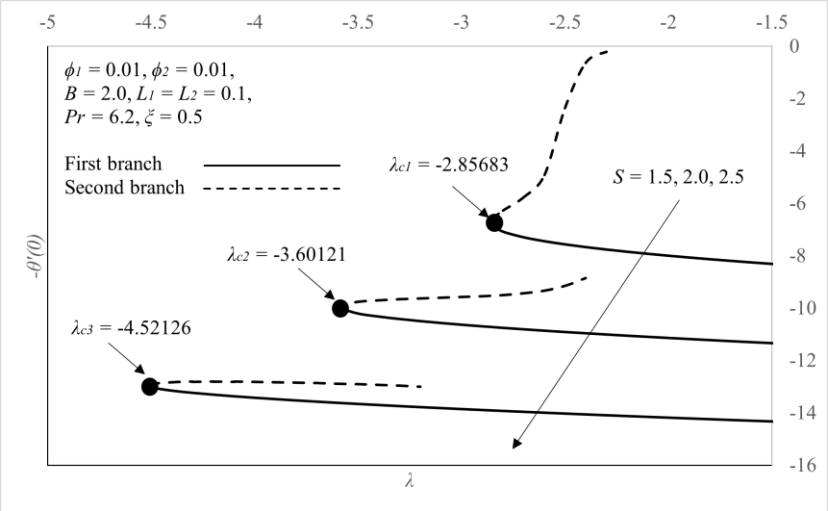

(b) Nusselt number $Nu_x Re_x^{-1/2}$

Fig. 4. Impact of *S* parameter on $C_f Re_x^{1/2}$ and $Nu_x\ Re_x^{-1/2}$

The effect of variable viscosity parameter *B* on dimensionless velocity and temperature profiles, $f'(\eta)$ and $\theta(\eta)$, are visualised in Figure 5(a) and 5(b), respectively. It is conveyed that the boundary layer thickness increases. This implies that the temperature difference between the ambient fluid and the flow surface is higher before the intensification of *B*. In the pattern of temperature profiles, the second branch of the solution depicts an increment, while the first solution behaves conversely, with the thickness of the boundary layer decreasing and increasing simultaneously. Figure 6(a) and 6(b) then employed the $f'(\eta)$ and $\theta(\eta)$ against mixed convection parameter ξ, where two different patterns are observed in the dimensionless velocity profiles as both first and second branches of solutions experience an increment in thermal transmittance rate. This phenomenon is attributed to a significant temperature gradient, which impacts the buoyancy level and directly influences the fluid convection. Initially, buoyancy forces drive the fluid flow by possessing a favourable temperature gradient. However, as the temperature rises, both thickness of the boundary layer and temperature profile incline. Consequently, there is a decrease in the second branch of $f'(\eta)$and an acceleration in heating flow in $\theta(\eta)$. Figure 7(a) and 7(b) plotted suction parameter *S* against velocity and temperature profiles where a mixed pattern is observed as in Figure 7(a) while the branches of

temperature profiles declined according to *S* number. Prior to this, a brief description can be made that the suction on boundary layer quickens the motion of hybrid nanoparticle and decrease the velocity gradient at the surface. The impact of suction is, simultaneously, triggering the buoyancy forces which lead to the movement of heated fluid towards the wall and created a delay in velocity and temperature gradients, hence occurring most solutions in both profiles to decrease.

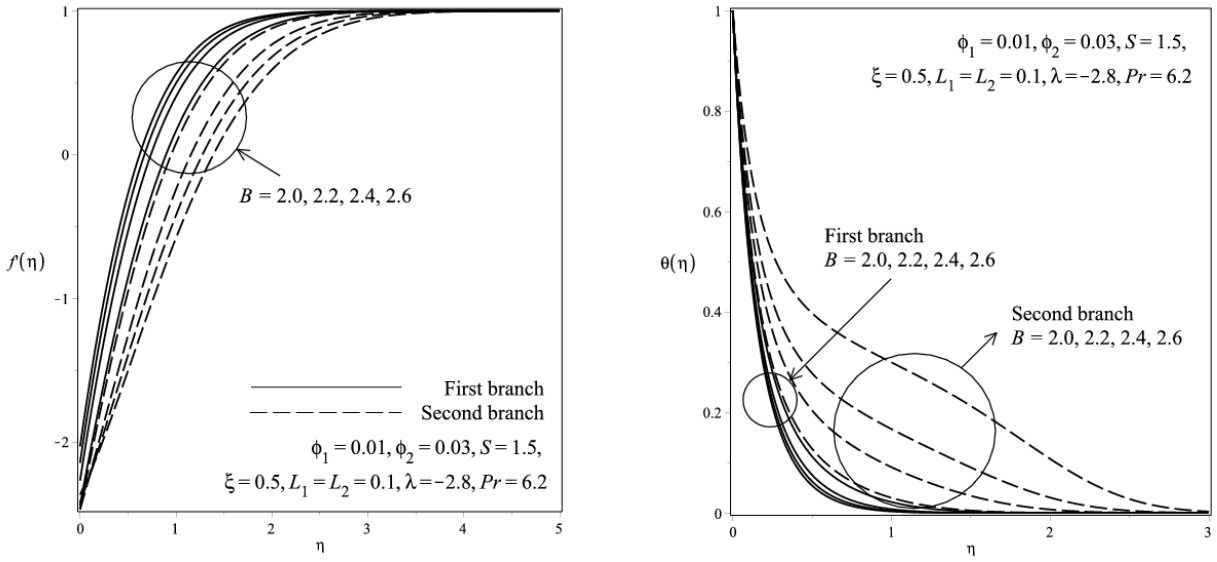

(a) Velocity profiles $f'(\eta)$ (b) Temperature profiles $\theta(\eta)$

Fig. 5. Impact of viscosity parameter *B* on flow profiles

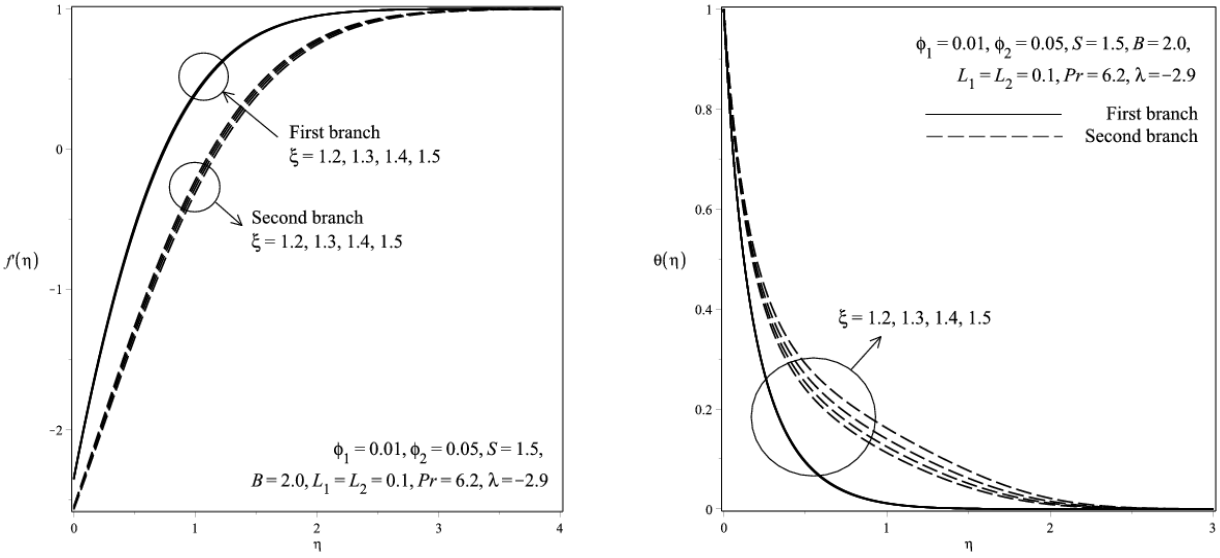

(a) Velocity profiles $f'(\eta)$ (b) Temperature profiles $\theta(\eta)$

Fig. 6. Impact of mixed convection parameter ξ on flow profiles

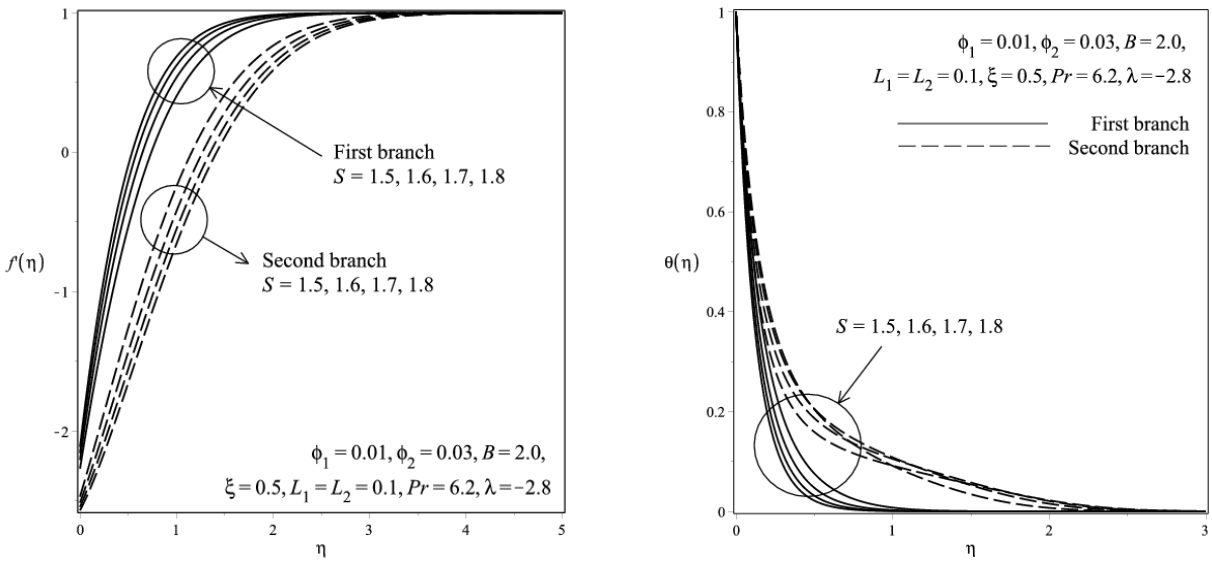

(a) Velocity profiles $f'(\eta)$ (b) Temperature profiles $\theta(\eta)$

Fig. 7. Impact of suction parameter *S* on flow profiles

Figure 8(a) and 8(b) determined the impact of shrinking parameter λ on the dimensionless profiles of velocity $f'(\eta)$ and temperature $\theta(\eta)$, accordingly. The lowest temperature in the first branch is conceived prior to the highest number of λ, while the other solutions in both profiles possessed both incline and decline. This can be explained due to the hybridity in the shrinking surface boosted the velocity distribution but dragged away the first branch of heat transfer rate.

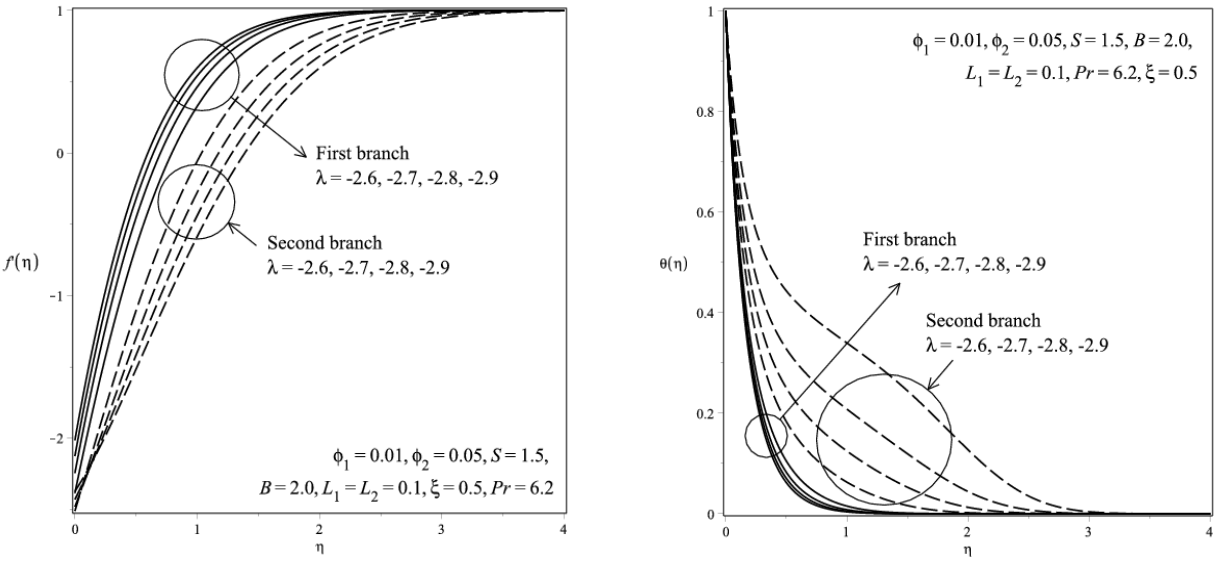

(a) Velocity profiles $f'(\eta)$ (b) Temperature profiles $\theta(\eta)$

Fig. 8. Impact of shrinking parameter λ on flow profiles

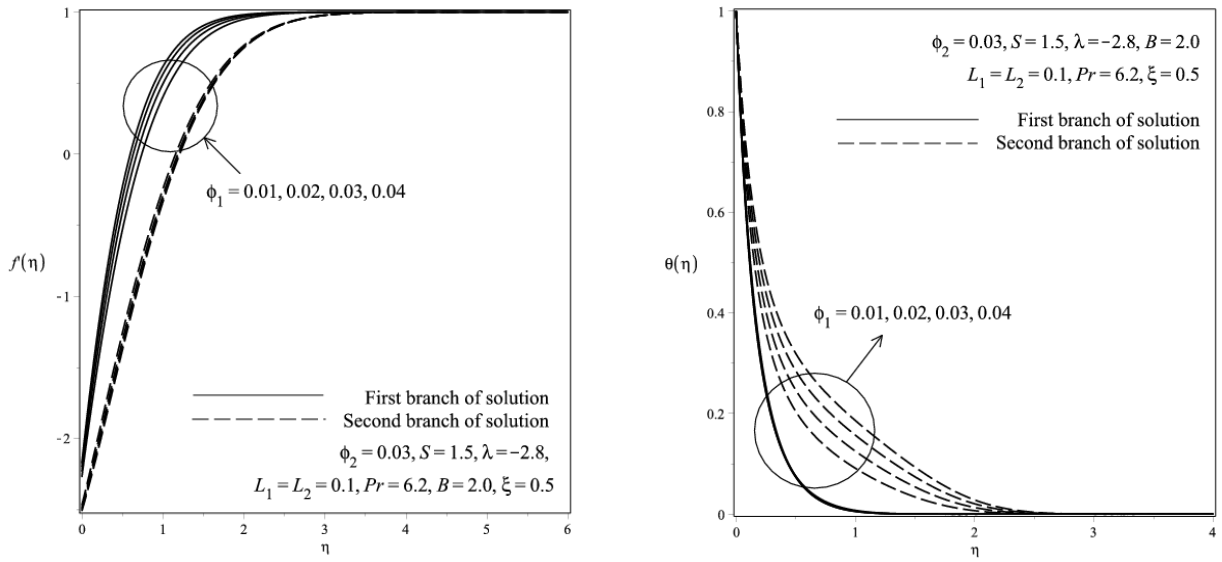

(a) Velocity profiles $f'(\eta)$ (b) Temperature profiles $\theta(\eta)$

Fig. 9. Impact of Ag-nanoparticle volume fraction ϕ_1 on flow profiles

Further, all solutions in velocity and temperature profiles are showing an enhancement as presented in Figure 9(a) and 9(b), respectively, versus the Ag-nanoparticle volume fraction ϕ_1. Physically, the development of viscous forces in the nanofluid was triggered by each additional number of nanoparticle volume fraction ϕ. As a result of the resistance engendered between the fluid particles, the heat transfer rate in temperature profiles increased while the velocity of the fluid particles decreased. Figure 10(a) and 10(b) then emphasized the flow profiles against second-order velocity slip L_2, while Figure 11 portrayed the influence of Prandtl number *Pr* on temperature distribution profiles $\theta(\eta)$.

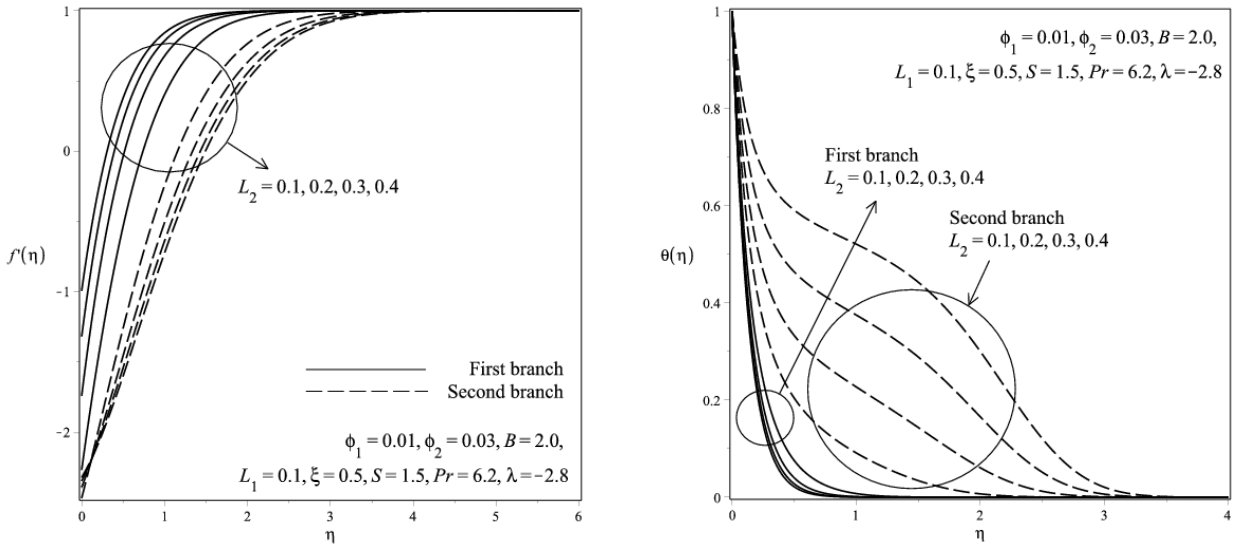

(a) Velocity profiles $f'(\eta)$ (b) Temperature profiles $\theta(\eta)$

Fig. 10. Impact of second-order velocity slip parameter L_2on flow profiles

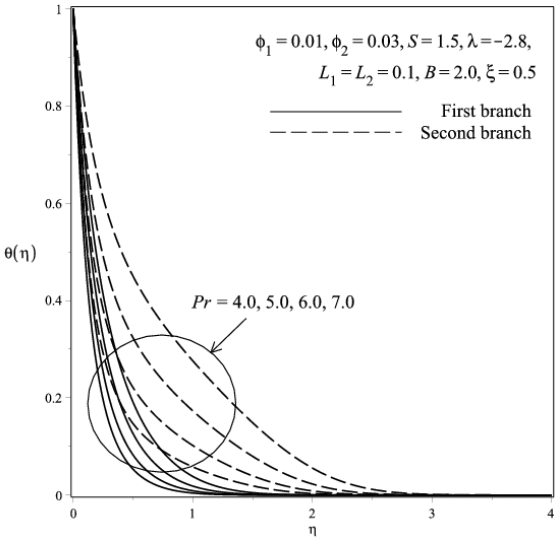

Fig. 11. Impact of Prandtl number *Pr* on temperature profiles $\theta(\eta)$

Based on Figure 10(a) and 10(b), most solutions exhibit a decreasing trend before experiencing an increase in fluid motion resistance due to L_2. Naturally, velocity and temperature distributions at a distance from the wall show a positive tendency. However, as the number of L_2 increases, the fluid flow and momentum boundary layer thicknesses are delayed due to the resistance of fluid motion. This justifies the decrement behaviour in Figure 10(a) and 10(b). From Figure 11, the $\theta(\eta)$ decreases significantly with higher *Pr* number, as it can reduce thermal diffusivity and weakens heat diffusion inside the fluid. Figure 12(a) and 12(b) then present the percentage of heat transmittance rate within the mono- and hybrid-nanofluids flow, considering Ag-$\phi_1 = 5\%$ and $0\% \leq \mathrm{CuO} - \phi_2 \leq 5\%$. It is evident that the percentage of heat transfer rate for mono-nanofluid is the lowest compared to the hybrid nanofluid. The heat transmittance rate difference in Figure 12(b) shows a gap of 13.89%, whereas the heat transfer difference rate between mono- and hybrid-nanofluid in Figure 12(a) slightly increases by 1.79%. Therefore, it is worth concluding that each increasing number of Ag-ϕ_1 results in a consistent rate compared to CuO-ϕ_2.

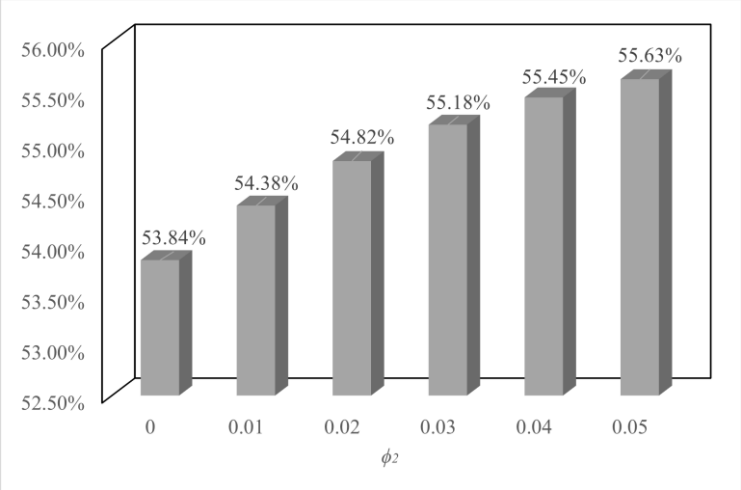

(a) Ag-$\phi_1 = 5\%$ and $0\% \leq \mathrm{CuO} - \phi_2 \leq 5\%$

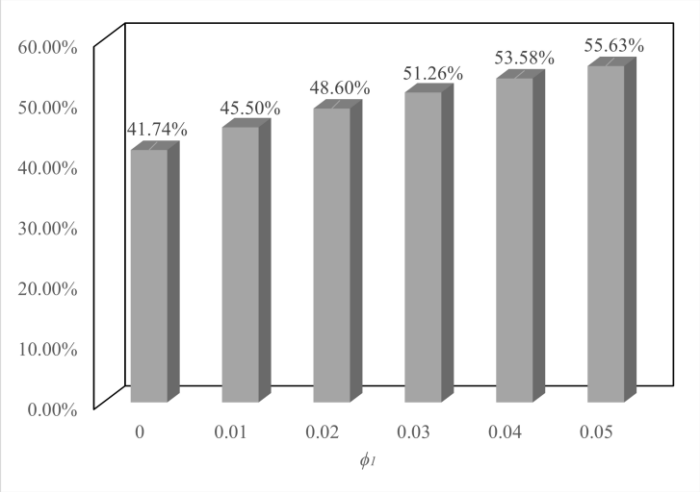

(a) CuO-$\phi_2 = 5\%$ and $0\% \leq$ Ag $- \phi_1 \leq 5\%$

Fig. 12. Heat transfer rate for mono- and hybrid-nanofluids

4. Stability Analysis

4.1 Mathematical Modelling for Stability Analysis

Stability analysis is conducted to distinguish the realizable physical solution between two branches of solutions associated with the shrinking parameter λ. To assess this condition, Weidman *et al.,* [46] and Merkin [47] proposed employing Eq. (2)-(4) in an unsteady state while keeping Eq. (1) constant. Prior to this, a new dimensionless time variable in the form of τ is introduced along with the similarity variables in Eq. (6)

$$u = cx\, f'(\eta), v = -\sqrt{c\nu_f} f(\eta), \theta = \frac{T-T_\infty}{T_w-T_\infty}, \eta = \sqrt{\frac{c}{\nu_f}} y, \tau = ct, \tag{14}$$

where *t* represents time. In general cases, steady flow occurs when the flow parameters at any point in the fluid remain constant over time. However, unsteady flow can occur when the flow parameters, such as velocity, pressure, and density, are time-dependent and subjected to time-varying boundary conditions, oscillatory motions, or transient disturbances, see Bakar *et al.,* [48]. Thus, with the consideration of our unsteady mathematical models and Eq. (14), we have

$$(1 - B\theta) D_1 \frac{\partial^3 f}{\partial \eta^3} + f \frac{\partial^2 f}{\partial \eta^2} - \left(\frac{\partial f}{\partial \eta}\right)^2 + 1 + D_2 \xi \theta - \frac{\partial^2 f}{\partial \tau \partial \eta} = 0, \tag{15}$$

$$D_3 \frac{\partial^2 \theta}{\partial \eta^2} + Pr\, f \frac{\partial \theta}{\partial \eta} + \frac{(1-B\theta)}{D_4} \left(\frac{\partial^2 f}{\partial \eta^2}\right)^2 - \frac{\partial \theta}{\partial \tau} = 0, \tag{16}$$

with the boundary conditions of

$$f(0,\tau) = S, \frac{\partial f(0,\tau)}{\partial \eta} = \lambda + L_1 \frac{\partial^2 f}{\partial \eta^2} + L_2 \frac{\partial^3 f}{\partial \eta^3}, \theta(0,\tau) = 1 \text{ at } \eta = 0,$$
$$\frac{\partial f(\tau,\eta)}{\partial \eta} \to 1, \theta(\tau,\eta) \to 0\ as\ \eta \to \infty. \tag{17}$$

The temporal stability analysis is then proposed as, see Weidman *et al.,* [46] and Merkin [47]

$$f(\eta,\tau) = f_0(\eta) + e^{-\varepsilon\tau}F(\eta),\ \theta(\eta,\tau) = \theta_0(\eta) + e^{-\varepsilon\tau}G(\eta). \tag{18}$$

Here f_0 and θ_0 are the small relatives of $F(\eta)$ and $G(\eta)$, accordingly, and ε denotes the elusive eigenvalue parameter, signifying the growth or decay rate of a disturbance. Eigenvalues play a pivotal role in discerning the stability of a fixed point within a solution. If a solution's fixed point is stable and subjected to initial disturbances, it will eventually return to its original position and remain there, as elaborated by Abu Bakar *et al.,* [49], Bakar *et al.,* [50] and Ismail *et al.,* [51]. The solution of eigenvalues provides an infinite set of $\varepsilon_1 < \varepsilon_2 < \varepsilon_3 <\ldots$, where the negative or positive numbers of ε represent the rate of expansion or deterioration of a disturbance rate. For instance, a positive number of ε indicates a decaying of the disturbance growth, resulting in a stable solution; and vice versa.

Further, the following linearized equations are obtained by adopting Eq. (18) into Eq. (15)-(17) such as the following

$$(1-BG)D_1F''' - f_0F'' + f_0''F - 2f_0'F' + D_2\xi G + \varepsilon F' = 0, \tag{19}$$

$$D_3G'' + Pr\left(f_0G' + \theta_0'F\right) + 2\left(\frac{1-BG}{D_4}\right)f_0''F'' + \varepsilon G = 0, \tag{20}$$

prior to the boundary conditions at

$$\begin{aligned} &F(0) = 0, F'(0) = L_1F''(0) + L_2F'''(0), G(0) = 0 \text{ when } \eta = 0 \\ &F'(\infty) \to 0, G(\infty) \to 0 \text{ when } \eta \to \infty. \end{aligned} \tag{21}$$

Later, Harris *et al.,* [52] emphasized that the condition of $F'(\eta) \to 0$ in Eq. (21) has been set at rest and replaced with the condition of $F''(\eta) = 1$ as $\eta \to \infty$.

4.2 Smallest Number of Eigenvalue ε

The bvp4c solver in MATLAB software is utilized to compute the smallest eigenvalue ε as described by Eq. (19)-(21). Specifically, bvp4c is a finite different code that employs the three-stage Lobatto Illa formula. This collocation formula provides a continuous solution in fourth-order accuracy within the uniform integration interval. Before obtaining the continuous polynomial solution, error control and selection of mesh number rely on this approach, as emphasized by Kierzenka and Shampine [53]. As a result, Table 4 presents a comparison of the smallest eigenvalue ε for two different amounts of hybrid nanoparticles volume fraction between Ag and CuO, while the list of ε number series against second-order velocity slip L_2 and mixed convection parameter ξ are presented in Table 5 and 6, respectively. A series of positive amounts are observed in all first branch of solution, while the second solution is distinguished to be in a series of negative numbers as can be noticed in these three tables. Thus, from the definition of eigenvalue ε, a firm conclusion can be drawn as the first branch is stable and the second solution is unstable.

Table 4
Two amount of hybrid nanoparticles and smallest eigenvalue ε

ϕ_1	ϕ_2	λ	ε	
			First branch of solution	Second branch of solution
5%	1%	-2.5	1.40713	-1.16439
		-2.6	0.85281	-0.63387
		-2.7	0.44823	-0.21172
	5%	-2.7	1.70310	-1.42352
		-2.8	1.28013	-0.86708
		-2.9	0.87577	-0.44671

Consideration of S = 1.5, $L_1 = L_2 = 0.1$, Pr = 6.2, $\xi = 0.5$ and B = 2.0.

Table 5
Second-order velocity slip L_2 and smallest eigenvalue ε

L_2	λ	ε	
		First branch of solution	Second branch of solution
0.2	-2.7	1.92483	-1.02923
	-2.8	1.59629	-0.79482
0.4	-2.8	2.49721	-1.23740
	-2.9	2.20880	-0.84545

Consideration of $\phi_1 = 1\%$, $\phi_2 = 5\%$, S = 1.5, $L_1 = 0.1$, Pr = 6.2, $\xi = 0.5$ and B = 2.0.

Table 6
Mixed convection parameter ξ and smallest eigenvalue ε

ξ	λ	ε	
		First branch of solution	Second branch of solution
1.5	-2.88	1.32458	-0.83726
	-2.98	1.13375	-0.63131
2.5	-3.05	1.69360	-0.96888
	-3.15	1.55508	-0.89545

Consideration of $\phi_1 = 1\%$, $\phi_2 = 5\%$, S = 1.5, $L_1 = L_2 = 0.1$, Pr = 6.2 and B = 2.0.

5. Conclusions

A steady, two-dimensional flow of hybrid Ag-CuO/H_2O nanofluid with the effect of second-order velocity slip and variable viscosity on mixed convection flow past a permeable shrinking stagnation-point region is thoroughly scrutinized in this current work. Two nanoparticles of Ag (silver) and CuO (copper oxide) are dispersed in the water to form the condition of hybrid nanofluid. The current findings in this study are possessed based on the rendered system of ODEs from a non-linear PDEs via similarity transformation method, which then are employed in shooting technique and bvp4c solver in Maple and MATLAB software, accordingly. The performing parameters – specifically nanoparticle volume fraction ϕ, shrinking parameter λ, variable viscosity parameter B, suction parameter S, second-order velocity slip L_2 and mixed convection parameter ξ are found to significantly affected the flow field. The final conclusions that can be drawn from this work are

i) Two branches of solutions are possessed prior to the shrinking surface $\lambda < 0$.

ii) The range of λ_c is significantly expanded as the number of CuO-nanoparticle-ϕ_2, suction parameter *S* and second-order velocity slip L_2 increase.

iii) Velocity profiles distribution is found to be align with Ag-nanoparticle-ϕ_1 and variable viscosity parameter *B*, while behaved conversely with second-order velocity slip L_2. Prior to the influence of shrinking parameter λ, suction parameter *S* and mixed convection parameter ξ, both solutions of velocity profiles performed mixed patterns.

iv) Temperature profiles distribution showed an increment for both branches of solutions against mixed convection parameter ξ and Ag-nanoparticle-ϕ_1. In the meantime, mixed behaviours are observed for variable viscosity parameter *B*, second-order velocity slip L_2 and shrinking parameter λ, while thermal profiles are declining with conjunction of suction parameter *S* and Prandtl number *Pr*.

v) Stability analysis is performed on the mathematical model due to dual solutions, and the first branch showed the most stable compared to the second branch as time evolved.

In conclusion, this research aims to shed light on the interplay between hybrid nanofluid dynamics, second-order velocity slip, and variable viscosity, contributing valuable insights to the field of mixed convection studies. The integration of Ag-CuO nanoparticles with H_2O offers exciting possibilities for various technological and biomedical applications. By presenting numerical outcomes and data analysis, it is hope that this research presents the understanding of mixed convection flow with hybrid nanofluid in practical engineering and scientific domains.

Declaration Statement

The authors declare that there are no competing interests or personal affiliations that could influence the content of this work.

Acknowledgements

The authors gratefully acknowledge and thank to Takasago Engineering Co. Ltd. through the grant number 4B732, as well as to Universiti Teknologi Malaysia (UTM), Universiti Putra Malaysia (UPM) and Ministry of Higher Education Malaysia (MOHE).

References

[1] Choi, S. US, and Jeffrey A. Eastman. *Enhancing thermal conductivity of fluids with nanoparticles*. No. ANL/MSD/CP-84938; CONF-951135-29. Argonne National Lab.(ANL), Argonne, IL (United States), 1995.

[2] Suresh, S., K. P. Venkitaraj, P. Selvakumar, and M. Chandrasekar. "Synthesis of Al2O3–Cu/water hybrid nanofluids using two step method and its thermo physical properties." *Colloids and Surfaces A: Physicochemical and Engineering Aspects* 388, no. 1-3 (2011): 41-48. https://doi.org/10.1016/j.colsurfa.2011.08.005

[3] Devi, SP Anjali, and S. Suriya Uma Devi. "Numerical investigation of hydromagnetic hybrid Cu–Al2O3/water nanofluid flow over a permeable stretching sheet with suction." *International Journal of Nonlinear Sciences and Numerical Simulation* 17, no. 5 (2016): 249-257. https://doi.org/10.1515/ijnsns-2016-0037

[4] Usman, M., M. Hamid, T. Zubair, Rizwan Ul Haq, and Wei Wang. "Cu-Al2O3/Water hybrid nanofluid through a permeable surface in the presence of nonlinear radiation and variable thermal conductivity via LSM." *International Journal of Heat and Mass Transfer* 126 (2018): 1347-1356. https://doi.org/10.1016/j.ijheatmasstransfer.2018.06.005

[5] Afridi, Muhammad Idrees, Tawfeeq Abdullah Alkanhal, Muhammad Qasim, and Iskander Tlili. "Entropy generation in Cu-Al2O3-H2O hybrid nanofluid flow over a curved surface with thermal dissipation." *Entropy* 21, no. 10 (2019): 941. https://doi.org/10.3390/e21100941

[6] Yahaya, Rusya Iryanti, Norihan M. Arifin, Roslinda Nazar, and Ioan Pop. "Flow and heat transfer past a permeable stretching/shrinking sheet in Cu− Al2O3/water hybrid nanofluid." *International Journal of Numerical Methods for Heat & Fluid Flow* 30, no. 3 (2020): 1197-1222. https://doi.org/10.1108/HFF-05-2019-0441

[7] Bakar, Shahirah Abu, Norihan Md Arifin, Norfifah Bachok, and Fadzilah Md Ali. "Effect of thermal radiation and MHD on hybrid Ag–TiO2/H2O nanofluid past a permeable porous medium with heat generation." *Case Studies in Thermal Engineering* 28 (2021): 101681. https://doi.org/10.1016/j.csite.2021.101681

[8] Abbas, Nadeem, S. Nadeem, Anber Saleem, M. Y. Malik, Alibek Issakhov, and Fahd M. Alharbi. "Models base study of inclined MHD of hybrid nanofluid flow over nonlinear stretching cylinder." *Chinese Journal of Physics* 69 (2021): 109-117. https://doi.org/10.1016/j.cjph.2020.11.019

[9] Gul, Taza, Kashifullah, M. Bilal, Wajdi Alghamdi, M. Imran Asjad, and Thabet Abdeljawad. "Hybrid nanofluid flow within the conical gap between the cone and the surface of a rotating disk." *Scientific Reports* 11, no. 1 (2021): 1180. https://doi.org/10.1038/s41598-020-80750-y

[10] Hussain, Azad, Ali Hassan, Qasem Al Mdallal, Hijaz Ahmad, Aysha Rehman, Mohamed Altanji, and Mubashar Arshad. "Heat transport investigation of magneto-hydrodynamics (SWCNT-MWCNT) hybrid nanofluid under the thermal radiation regime." *Case Studies in Thermal Engineering* 27 (2021): 101244. https://doi.org/10.1016/j.csite.2021.101244

[11] Muhammad, Khursheed, T. Hayat, A. Alsaedi, and B. Ahmad. "Melting heat transfer in squeezing flow of basefluid (water), nanofluid (CNTs+ water) and hybrid nanofluid (CNTs+ CuO+ water)." *Journal of Thermal Analysis and Calorimetry* 143 (2021): 1157-1174. https://doi.org/10.1007/s10973-020-09391-7

[12] Rashidi, Mohammad Mehdi, Maryam Sadri, and Mikhail A. Sheremet. "Numerical simulation of hybrid nanofluid mixed convection in a lid-driven square cavity with magnetic field using high-order compact scheme." *Nanomaterials* 11, no. 9 (2021): 2250. https://doi.org/10.3390/nano11092250

[13] Hussain, S., Sameh E. Ahmed, and T. Akbar. "Entropy generation analysis in MHD mixed convection of hybrid nanofluid in an open cavity with a horizontal channel containing an adiabatic obstacle." *International Journal of Heat and Mass Transfer* 114 (2017): 1054-1066. https://doi.org/10.1016/j.ijheatmasstransfer.2017.06.135

[14] Jarray, Amira, Zouhaier Mehrez, and Afif El Cafsi. "Mixed convection Ag-MgO/water hybrid nanofluid flow in a porous horizontal channel." *The European Physical Journal Special Topics* 228, no. 12 (2019): 2677-2693.. https://doi.org/10.1140/epjst/e2019-900068-8

[15] Rostami, Mohammadreza Nademi, Saeed Dinarvand, and Ioan Pop. "Dual solutions for mixed convective stagnation-point flow of an aqueous silica–alumina hybrid nanofluid." *Chinese journal of physics* 56, no. 5 (2018): 2465-2478.. https://doi.org/10.1016/j.cjph.2018.06.013

[16] Khan, M. Riaz, Kejia Pan, Arif Ullah Khan, and S. Nadeem. "Dual solutions for mixed convection flow of SiO2−Al2O3/water hybrid nanofluid near the stagnation point over a curved surface." *Physica A: Statistical Mechanics and its Applications* 547 (2020): 123959. https://doi.org/10.1016/j.physa.2019.123959

[17] Zainal, Nurul Amira, Roslinda Nazar, Kohilavani Naganthran, and Ioan Pop. "MHD mixed convection stagnation point flow of a hybrid nanofluid past a vertical flat plate with convective boundary condition." *Chinese Journal of Physics* 66 (2020): 630-644. https://doi.org/10.1016/j.cjph.2020.03.022

[18] Elsaid, Essam M., and Mohamed S. Abdel-Wahed. "Mixed convection hybrid-nanofluid in a vertical channel under the effect of thermal radiative flux." *Case Studies in Thermal Engineering* 25 (2021): 100913. https://doi.org/10.1016/j.csite.2021.100913

[19] Khashi'ie, Najiyah Safwa, Norihan M. Arifin, John H. Merkin, Rusya Iryanti Yahaya, and Ioan Pop. "Mixed convective stagnation point flow of a hybrid nanofluid toward a vertical cylinder." *International Journal of Numerical Methods for Heat & Fluid Flow* 31, no. 12 (2021): 3689-3710. https://doi.org/10.1016/j.cjph.2021.07.030

[20] Patil, P. M., and Madhavarao Kulkarni. "Analysis of MHD mixed convection in a Ag-TiO2 hybrid nanofluid flow past a slender cylinder." *Chinese Journal of Physics* 73 (2021): 406-419. https://doi.org/10.1108/HFF-11-2020-0725

[21] Roșca, Natalia C., Alin V. Roșca, and Ioan Pop. "Mixed convection flow of a hybrid nanofluid past a vertical wedge with thermal radiation effect." *International Journal of Numerical Methods for Heat & Fluid Flow* 32, no. 2 (2021): 806-824. https://doi.org/10.1108/HFF-03-2021-0155

[22] Gohar, Tahir Saeed Khan, Imran Khan, Taza Gul, and Muhammad Bilal. "Mixed convection and thermally radiative hybrid nanofluid flow over a curved surface." *Advances in Mechanical Engineering* 14, no. 3 (2022): 16878132221082848. https://doi.org/10.1177%2F16878132221082848

[23] Xia, Wei-Feng, Shafiq Ahmad, Muhammad Naveed Khan, Hijaz Ahmad, Aysha Rehman, Jamel Baili, and Tuan Nguyen Gia. "Heat and mass transfer analysis of nonlinear mixed convective hybrid nanofluid flow with multiple slip boundary conditions." *Case Studies in Thermal Engineering* 32 (2022): 101893. https://doi.org/10.1016/j.csite.2022.101893

[24] Zhu, Jing, Dan Yang, Liancun Zheng, and Xinxin Zhang. "Effects of second order velocity slip and nanoparticles migration on flow of Buongiorno nanofluid." *Applied mathematics letters* 52 (2016): 183-191. https://doi.org/10.1016/j.aml.2015.09.003

[25] Zhu, Jing, Liu Zheng, Liancun Zheng, and Xinxin Zhang. "Second-order slip MHD flow and heat transfer of nanofluids with thermal radiation and chemical reaction." *Applied Mathematics and Mechanics* 36, no. 9 (2015): 1131-1146. https://doi.org/10.1007/s10483-015-1977-6

[26] Roşca, Alin V., Natalia C. Roşca, and Ioan Pop. "Mixed convection stagnation point flow of a hybrid nanofluid past a vertical flat plate with a second order velocity model." *International Journal of Numerical Methods for Heat & Fluid Flow* 31, no. 1 (2021): 75-91. https://doi.org/10.1108/HFF-03-2020-0152

[27] Yan, Liang, Sumera Dero, Ilyas Khan, Irshad Ali Mari, Dumitru Baleanu, Kottakkaran Sooppy Nisar, El-Sayed M. Sherif, and Hany S. Abdo. "Dual solutions and stability analysis of magnetized hybrid nanofluid with joule heating and multiple slip conditions." *Processes* 8, no. 3 (2020): 332. https://doi.org/10.3390/pr8030332

[28] Tulu, Ayele, and Wubshet Ibrahim. "Effects of Second-Order Slip Flow and Variable Viscosity on Natural Convection Flow of (CNTs-Fe_3O_4)/Water Hybrid Nanofluids due to Stretching Surface." *Mathematical Problems in Engineering* 2021 (2021): 1-18. https://doi.org/10.1155/2021/8407194

[29] Waini, Iskandar, Anuar Ishak, Teodor Groşan, and Ioan Pop. "Mixed convection of a hybrid nanofluid flow along a vertical surface embedded in a porous medium." *International Communications in Heat and Mass Transfer* 114 (2020): 104565. https://doi.org/10.1016/j.icheatmasstransfer.2020.104565

[30] Gul, Hina, Muhammad Ramzan, Jae Dong Chung, Yu-Ming Chu, and Seifedine Kadry. "Multiple slips impact in the MHD hybrid nanofluid flow with Cattaneo–Christov heat flux and autocatalytic chemical reaction." *Scientific Reports* 11, no. 1 (2021): 14625. https://doi.org/10.1038/s41598-021-94187-4

[31] Abu Bakar, Shahirah, Nur Syahirah Wahid, Norihan Md Arifin, and Najiyah Safwa Khashi'ie. "The flow of hybrid nanofluid past a permeable shrinking sheet in a Darcy–Forchheimer porous medium with second-order velocity slip." *Waves in Random and Complex Media* (2022): 1-18. https://doi.org/10.1080/17455030.2021.2020375

[32] Botmart, Thongchai, U. S. Mahabaleshwar, and A. B. Vishalakshi. "Heat transfer and hybrid nanofluid flow over a porous stretching/shrinking sheet with Brinkmann model and multiple slips." (2022). https://doi.org/10.21203/rs.3.rs-1385643/v1

[33] Lone, Showkat Ahmad, Maryam Ahmed Alyami, Anwar Saeed, Abdullah Dawar, Poom Kumam, and Wiyada Kumam. "MHD micropolar hybrid nanofluid flow over a flat surface subject to mixed convection and thermal radiation." *Scientific Reports* 12, no. 1 (2022): 17283. https://doi.org/10.1038/s41598-022-21255-8

[34] Asghar, Adnan, Abdul Fattah Chandio, Zahir Shah, Narcisa Vrinceanu, Wejdan Deebani, Meshal Shutaywi, and Liaquat Ali Lund. "Magnetized mixed convection hybrid nanofluid with effect of heat generation/absorption and velocity slip condition." *Heliyon* 9, no. 2 (2023). https://doi.org/10.1016/j.heliyon.2023.e13189

[35] Xie, Hongmei, Bin Jiang, Bo Liu, Qinghang Wang, Junyao Xu, and Fusheng Pan. "An investigation on the tribological performances of the SiO 2/MoS 2 hybrid nanofluids for magnesium alloy-steel contacts." *Nanoscale research letters* 11 (2016): 1-17. https://doi.org/10.1186/s11671-016-1546-y

[36] Takabi, Behrouz, and Saeed Salehi. "Augmentation of the heat transfer performance of a sinusoidal corrugated enclosure by employing hybrid nanofluid." *Advances in Mechanical Engineering* 6 (2014): 147059. https://doi.org/10.1155%2F2014%2F147059

[37] Ghalambaz, Mohammad, S. A. M. Mehryan, Ahmad Hajjar, and Ali Veismoradi. "Unsteady natural convection flow of a suspension comprising Nano-Encapsulated Phase Change Materials (NEPCMs) in a porous medium." *Advanced Powder Technology* 31, no. 3 (2020): 954-966. https://doi.org/10.1016/j.apt.2019.12.010

[38] Manjunatha, S., B. Ammani Kuttan, S. Jayanthi, Ali Chamkha, and B. J. Gireesha. "Heat transfer enhancement in the boundary layer flow of hybrid nanofluids due to variable viscosity and natural convection." *Heliyon* 5, no. 4 (2019). https://doi.org/10.1016/j.heliyon.2019.e01469

[39] Venkateswarlu, Bhumavarapu, and Panyam Venkata Satya Narayana. "Cu-Al2O3/H2O hybrid nanofluid flow past a porous stretching sheet due to temperatue-dependent viscosity and viscous dissipation." *Heat Transfer* 50, no. 1 (2021): 432-449. https://doi.org/10.1002/htj.21884 [40]

[40] Wu, Lin. "A slip model for rarefied gas flows at arbitrary Knudsen number." *Applied Physics Letters* 93, no. 25 (2008). https://doi.org/10.1063/1.3052923

[41] Acharya, Nilankush, Kalidas Das, and Prabir Kumar Kundu. "Outlining the impact of second-order slip and multiple convective condition on nanofluid flow: a new statistical layout." *Canadian Journal of Physics* 96, no. 1 (2018): 104-111. https://doi.org/10.1139/cjp-2017-0062

[42] Aly, Emad H., and Ioan Pop. "MHD flow and heat transfer over a permeable stretching/shrinking sheet in a hybrid nanofluid with a convective boundary condition." *International Journal of Numerical Methods for Heat & Fluid Flow* 29, no. 9 (2019): 3012-3038. https://doi.org/10.1108/HFF-12-2018-0794

[43] Abu Bakar, Shahirah, Norihan Md Arifin, Najiyah Safwa Khashi'ie, and Norfifah Bachok. "Hybrid nanofluid flow over a permeable shrinking sheet embedded in a porous medium with radiation and slip impacts." *Mathematics* 9, no. 8 (2021): 878. https://doi.org/10.3390/math9080878

[44] Waini, Iskandar, Anuar Ishak, and Ioan Pop. "Melting heat transfer of a hybrid nanofluid flow towards a stagnation point region with second-order slip." *Proceedings of the Institution of Mechanical Engineers, Part E: Journal of Process Mechanical Engineering* 235, no. 2 (2021): 405-415. https://doi.org/10.1177/0954408920961213
[45] Bachok, Norfifah, Anuar Ishak, and Ioan Pop. "Stagnation-point flow over a stretching/shrinking sheet in a nanofluid." *Nanoscale research letters* 6 (2011): 1-10. https://doi.org/10.1186/1556-276X-6-623
[46] Weidman, P. D., D. G. Kubitschek, and A. M. J. Davis. "The effect of transpiration on self-similar boundary layer flow over moving surfaces." *International journal of engineering science* 44, no. 11-12 (2006): 730-737. https://doi.org/10.1016/j.ijengsci.2006.04.005
[47] Merkin, J. H. "On dual solutions occurring in mixed convection in a porous medium." *Journal of engineering Mathematics* 20, no. 2 (1986): 171-179. https://doi.org/10.1007/BF00042775
[48] Bakar, S. A., N. M. Arifin, N. Bachok, and F. M. Ali. "Hybrid Nanofluid Flow in a Porous Medium with Second-Order Velocity Slip, Suction and Heat Absorption." *Malaysian J. Math. Sci* 16 (2022): 257-272. https://doi.org/10.47836/mjms.16.2.06
[49] Abu Bakar, Shahirah, Norihan Md Arifin, Fadzilah Md Ali, Norfifah Bachok, Roslinda Nazar, and Ioan Pop. "A stability analysis on mixed convection boundary layer flow along a permeable vertical cylinder in a porous medium filled with a nanofluid and thermal radiation." *Applied Sciences* 8, no. 4 (2018): 483. https://doi.org/10.3390/app8040483
[50] Bakar, Shahirah Abu, Norihan Md Arifin, Roslinda Nazar, Fadzilah Md Ali, Norfifah Bachok, and Ioan Pop. "The effects of suction on forced convection boundary layer stagnation point slip flow in a darcy porous medium towards a shrinking sheet with presence of thermal radiation: A stability analysis." *Journal of Porous Media* 21, no. 7 (2018). https://doi.org/10.1615/JPorMedia.2018019722
[51] Ismail, N. S., N. M. Ariffin, R. Nazar, and N. Bachok. "Stability analysis of stagnation-point flow and heat transfer over an exponentially shrinking sheet with heat generation." *Malaysian Journal of Mathematical Sciences* 13, no. 2 (2019): 107-122.
[52] Harris, S. D., D. B. Ingham, and I. Pop. "Mixed convection boundary-layer flow near the stagnation point on a vertical surface in a porous medium: Brinkman model with slip." *Transport in Porous Media* 77 (2009): 267-285. https://doi.org/10.1007/s11242-008-9309-6
[53] Kierzenka, Jacek, and Lawrence F. Shampine. "A BVP solver based on residual control and the Maltab PSE." *ACM Transactions on Mathematical Software (TOMS)* 27, no. 3 (2001): 299-316. https://doi.org/10.1145/502800.502801